An integrated cellulose aerogel evaporator with improved thermal management and reduced enthalpy of evaporation using a hierarchical coordinated control strategy

Jiaming Sun,[a,b, §] Rui Teng, [a,b, §] Jia Tan, [a,b] Mingcong Xu,[a,b] Chunhui Ma,[a,b] Wei Li,* [a, b] Shouxin Liu* [a, b]

[a] Key Laboratory of Bio-based Material Science and Technology of the Ministry of Education

[b] Engineering Research Center of Advanced Wooden Materials of the Ministry of Education, Northeast Forestry University, Harbin 150040, China

Corresponding Author: Wei Li (*Email: liwei820927@nefu.edu.cn)

Shouxin Liu (*Email: liushouxin@ nefu.edu.cn)

S1. Supplemental methods

S1.1. characterization

Scanning electron microscope (SEM) images were acquired on a Quanta 200 (American FEI Company). The contact angle was measured using Kruss Drop Shape Analyzer (Kruss Gmbh DSA255). The UV-vis-NIR spectra were obtained on a PerkinElmer Lambda 950 spectrophotometer. The optical absorption can be calculated as 100%-R%-T%. [1] The thermal conductivity of the aerogels was measured using a thermal analyzer (TPS 2500 S, Hot Disk, Sweden). DSC data was measured using Mettler 1100LF (Mettler Toledo, Gießen, Germany). A CEL-HXF300 xenon lamp (Beijing Education Au-light Co. Ltd., China) was used to simulate sunlight. The light intensity was determined using a CELNP2000 strong light power meter (Beijing Education Au-light Co. Ltd., China). The temperature of specimens was measured by an infrared (IR) thermometer (FLIR A35). The ion content in water was measured using an inductively coupled plasma optical emission spectrometer (ICP-OES) (730-ES, Varian, USA).

S1.2. Preparation of micro-fibrillated cellulose (MFC)

The kapok fibers were smashed by a pulverizer. Lignin was then removed by the acidified $NaClO_2$ method. Concretely, Kapok fibers were treated with a fixed proportion of CH_3COOH and $NaClO_2$ in a water bath at 80 °C for 2 h until the kapok fibers turn white. Then hemicellulose was removed with 4 wt% NaOH at 90 °C for 4 h. Finally, the sample was washed with distilled water to neutrality by filtration to obtain kapok fiber-based cellulose. The obtained kapok fiber-based cellulose was formulated into a 0.8% suspension and then ultrasonicated (JY98-IIID, Ningbo Scientz Biotechnology Co., Ltd., China) under 1200 W for 15 min in an ice/water bath to isolate the microfibers for obtaining micro-fibrillated cellulose.

S2. Calculation of solar evaporation efficiency

The evaporation efficiency under the solar simulator is calculated by Equation 1:

$$\eta = \frac{r_{net} r h_{lv}}{P_{in}} \quad (1)$$

where r_{net} is the net evaporation rate (kg m^{-2} h^{-1}), h_{lv} represents the latent enthalpy of the liquid-vapor phase change of water (kJ kg^{-1}), and P_{in} denotes the incident solar irradiation power (kW m^{-2}). The net evaporation rate r is calculated by the following Equation 2:

$$r_{net} = r_{aerogel} - r_{dark} \quad (2)$$

where $r_{aerogel}$ is the total mass change evaporating from the aerogel (kg m^{-2} h^{-1}) and can be read in Figure 4. r_{dark} is the dark environment evaporation rate without sun irradiation (kg m^{-2} h^{-1}). r_{dark} can be obtained by evaporation experiment in a dark environment.

$r_{aerogel}$ can be calculated by the following Equation 3:

$$r_{aerogel} = \frac{m_{total} - m_{shadow}}{t \times S_{aerogel}} \quad (3)$$

where m_{total} is the total mass change within the box (kg). It can be obtained by electronic balance.

m_{shadow} can be estimated by the following Equation 4 through a blank water evaporating experiment:

$$m_{shadow} = \frac{m_{blank}}{S_{shadow} + S_{aerogel}} \times S_{shadow}. \quad (4)$$

Where m_{blank} is the total mass change within the box (kg) without an aerogel in a blank water evaporating experiment.

h_{lv} can be obtained by DSC in Table S2.

S3. Estimation of heat loss

The energy losses of HCE-T$_2$ with an exposed area of 0.0012 m^2 under 1 sun irradiation is calculated. The localized thermal energy at evaporator via photo-thermal conversion can be divided into five parts: energy consumption by water evaporator, loss of reflection on evaporator surface, heat radiation loss, heat conduction loss and heat convection loss. The detailed calculation of heat loss is analyzed as below [2,3].

Evaporator surface reflection loss

Considering the optical absorption of HCE-T$_2$ is about 97%, the reflect heat loss should be about 3%.

Radiation loss

The radiation loss of the evaporator is calculated by the Steafan-Boltzmann equation as the following Equations 5-6,

$$\Phi = A\varepsilon\sigma(T_1{}^4 - T_2{}^4) \quad (5)$$

$$Radiation\ loss = \frac{\Phi}{AC_{opt}q_i} = \frac{\varepsilon\sigma(T_1{}^4 - T_2{}^4)}{C_{opt}q_i} \quad (6)$$

Where Φ is the heat flux, ε is the emissivity of the absorbing surface (0.88), A represents the exposed area (m^2), σ is the Stefan-Boltzmann constant which is 5.67×10^{-8} J m^{-2} s^{-1} K^{-4}, T_1 is the surface temperature of HCE-T$_2$ (320.05K). T_2 is the adjacent environment temperature (296.55K). The radiation heat loss is 13.76% for the evaporator under 1 sun irradiation.

Conduction

Although the thermal-insulation layer is set to prevent the heat loss to the bulk solution from conduction and convection, a portion heat loss conducted to bulk water might be occur via the hydrophilic water pumping layer. The conduction loss is calculated based on the bulk water absorption heat Q as the following Equations 7-8,

$$Q = Cm\Delta T \quad (7)$$

$$Conduction\ loss = \frac{Q}{AC_{opt}q_i\Delta t} = \frac{Cm\Delta T}{AC_{opt}q_i\Delta t} \quad (8)\_$$

Where Q represents the heat flux, C represents the specific heat capacity of water (4200 J °C^{-1} kg^{-1}), m is the bulk water used in the experiment (~0.01kg), ΔT is the temperature

change of the bulk water during the Δt (4.5 °C after 3600 s). The conduction heat loss is 4.37% in this experiment.

Convection

The convection loss is calculated based on the Newton's Law of Cooling as the following Equations 9-10,

$$\Psi = \xi A \Delta T \quad (9)$$

$$Convection\ loss = \frac{\Psi}{AC_{opt}q_i} = \frac{\xi \Delta T}{C_{opt}q_i} \quad (10)$$

Where Ψ is the heat flux, ξ is the convection heat transfer coefficient (2.24 J m^{-2} s^{-1} K^{-1}),[6] ΔT is the temperature difference between the surface temperature of the evaporator (320.05K) and the adjacent environment temperature (296.55K). The convective heat loss is 5.26% in this experiment.

In summary, the total heat loss for the HCE-T$_2$ under 1 sun irradiation is about 26.39%. Therefore, the total energy consumption of the five parts is about 73.61%, which is in good agreement with the experimental photo-thermal conversion efficiency 81.75%.
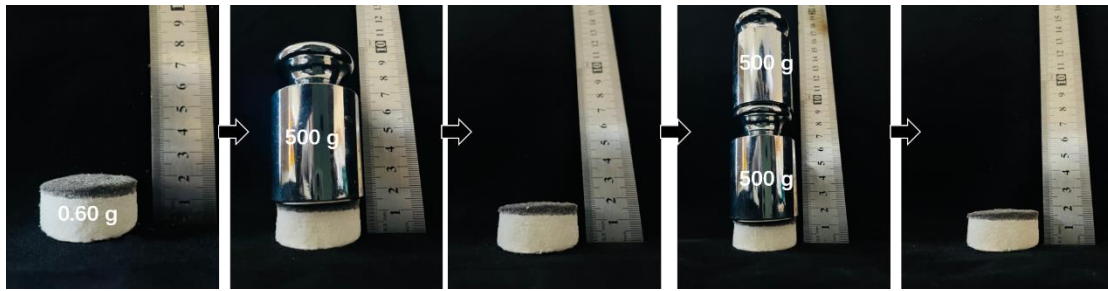
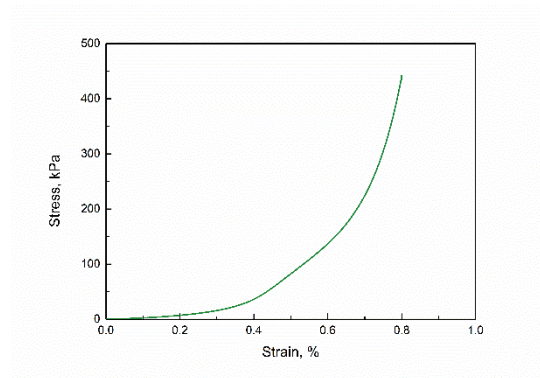**Figure S1** Images of HCE-T$_2$ specimen withstanding a load of 1.0 kg without any interlayer fracture.

Figure S2 Stress-strain curves of HCE-T$_2$

To verify the mechanical property of the sample, HCE-T$_2$ was firstly subjected to a press test with weights. As shown in Figure S1, HCE-T$_2$ was found to possess a high mechanical resistance. A 0.6 g of the HCE-T$_2$ could withstand 1666 times its own mass with a little densification but without interlayer fracture, suggesting the stability between layers and superior mechanical robustness. The strain-stress test further verified this conclusion. As shown in Figure S2, the compressive stress of HCE-T$_2$ was about 435 kPa under the strain of 80%. Video S1 showed that as the compressive stress increases, HCE-T$_2$ had a large deformation without collapse. Until the end of the test, three layers of HCE-T$_2$ still connected tightly. These experiments verified the steady combination between layers.
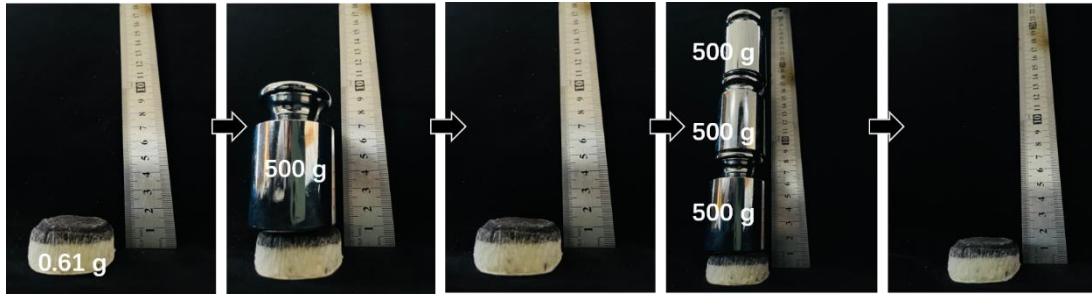
Figure S3 Images of the used specimen withstanding a load of 1.5 kg without any interlayer fracture.
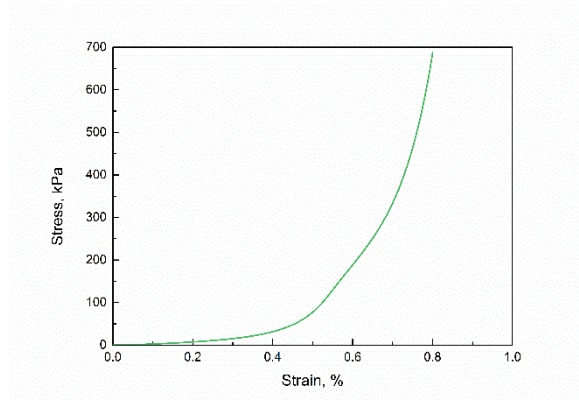

Figure S4 Stress-strain curves of the used specimen.

The sample that has been used in evaporation experiments was directly dried in the environment instead of freeze-drying. As shown in Figure S3, the used sample had a little deformation and shrank slightly after drying under ambient pressure. But the combination between layers is still tight. To verify the mechanical property of the sample, the sample was firstly subjected to a press test with weights. As shown in Figure S3, it was found to possess high mechanical resistance. A 0.61 g of the sample could withstand 2459 times its own mass with densification but without interlayer fracture, suggesting the stability between layers and superior mechanical robustness. The strain-stress test further verified this conclusion. As shown in Figure S4, the compressive stress of the used HCE-T_2 was about 685 kPa under the strain of 80%. The used HCE-T_2 have a higher compressive stress than that of HCE-T_2 because the used HCE-T_2 had more a NaCl content and the cellulose-based skeleton became tight after ambient pressure. Until the end of the test, three layers of the used HCE-T_2 still connected tightly. These experiments verified that the used sample also a good mechanical behavior.
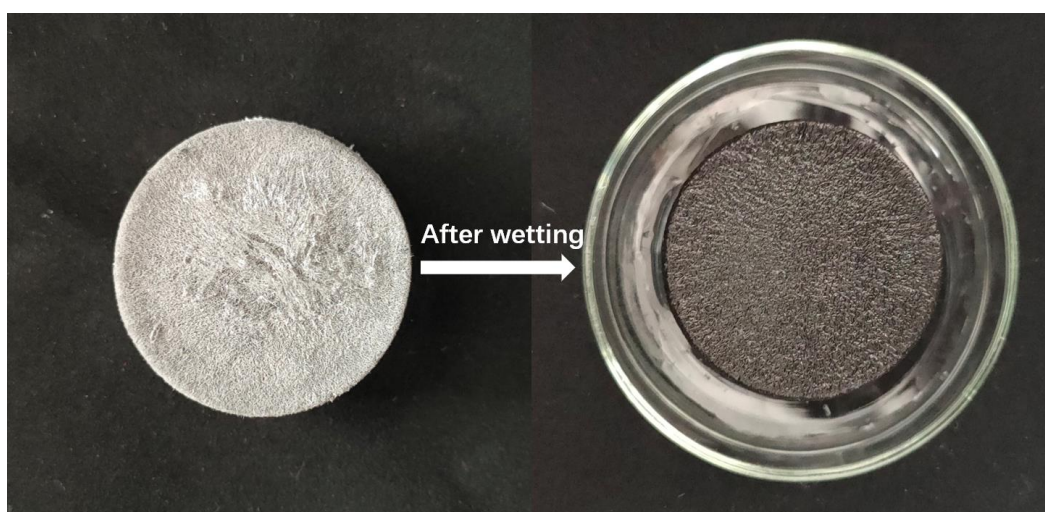
Figure S5 Digital photo of HCE-T$_2$ after wetting.

The color of the HCE-T$_2$ became darker after wetting because wetted surfaces effectively reduced surface scattering.
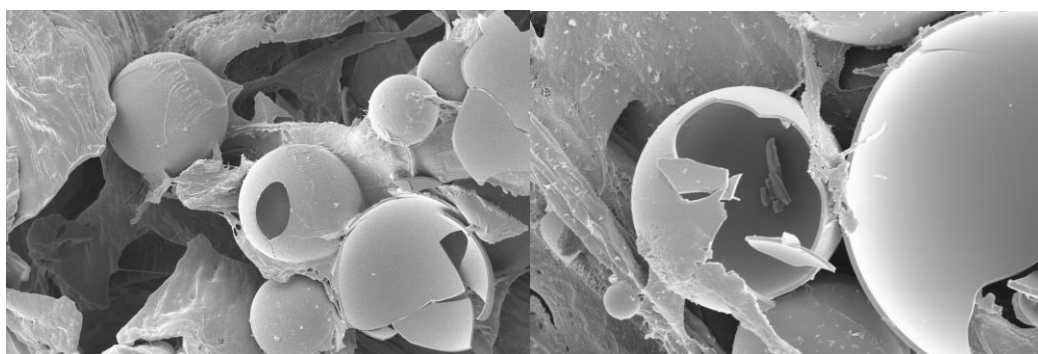

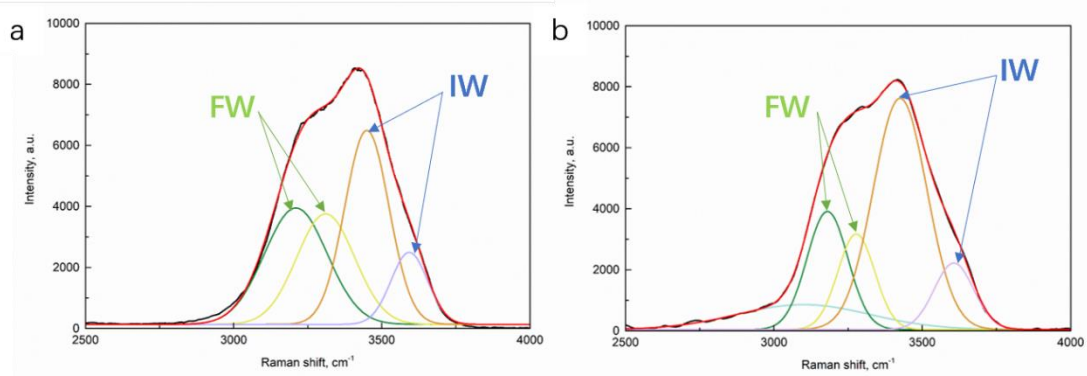**Figure S6** The SEM images of broken GBs. GBs have hollow structures.

Figure S7 Raman spectra of (a) 3.5wt% NaCl aqueous solution and (b) HCE-T$_2$

To prove the existence of different types of water molecules, the Raman spectra of (a) aqueous solution and (b) HCE-T$_2$ were fitted by four peaks through Gaussian function. As displayed in Figure S7, Raman spectra between 3200 and 3700 cm^{-1} were curve-fitted into four peaks at about 3200, 3401, 3500 and 3630 cm^{-1} [5]. The peaks of FW are located at 3200 and 3401 cm^{-1}, meaning that the FW forms four hydrogen bonds with adjacent hydrophilic group or water molecule. The IW with fewer hydrogen bonds displays two peaks, which are located at 3500 and 3630 cm^{-1}. They are aroused from the symmetric and asymmetric –OH stretching vibrations, respectively, due to the weak hydrogen bonds in water molecules. [6,7] The ratio of IW to FW in HCE-T$_2$ is obviously higher than that of pure water. Therefore, compared with pure water, the water in the aerogel has a higher proportion of IW, which contributes to the decrease in vaporization enthalpy for accelerating water evaporation.

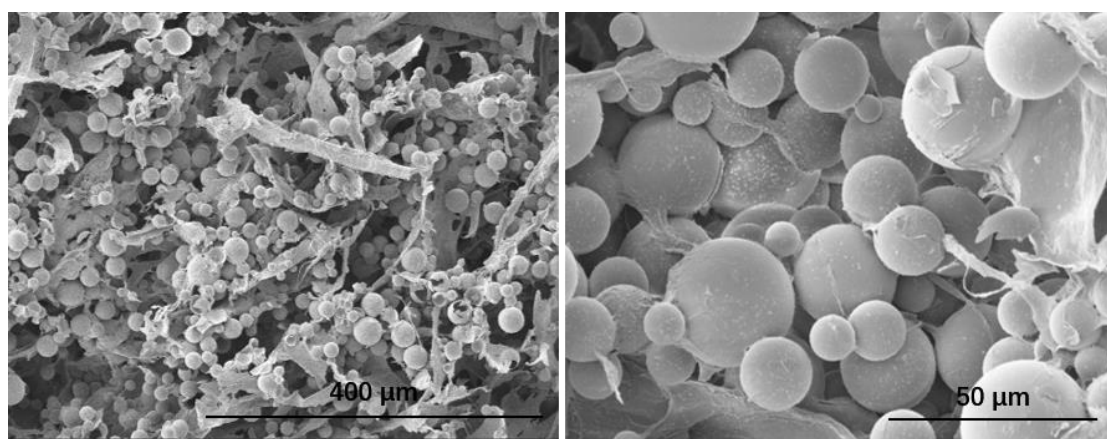**Figure S8** Left: Digital photo of HCE-T$_2$ during evaporation. Right: diagram of calculation area.

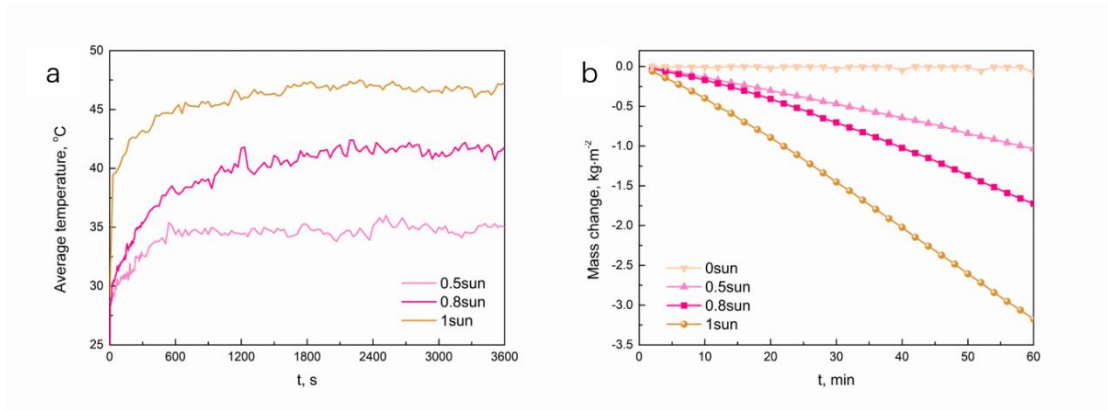**Figure S9** The SEM images of HCE-T$_3$.

Figure S10 (a) The surface temperatures and (b) cumulative mass changes of specimens over time under different sun radiation (The testing temperature and RH was 19ºC and 39%).
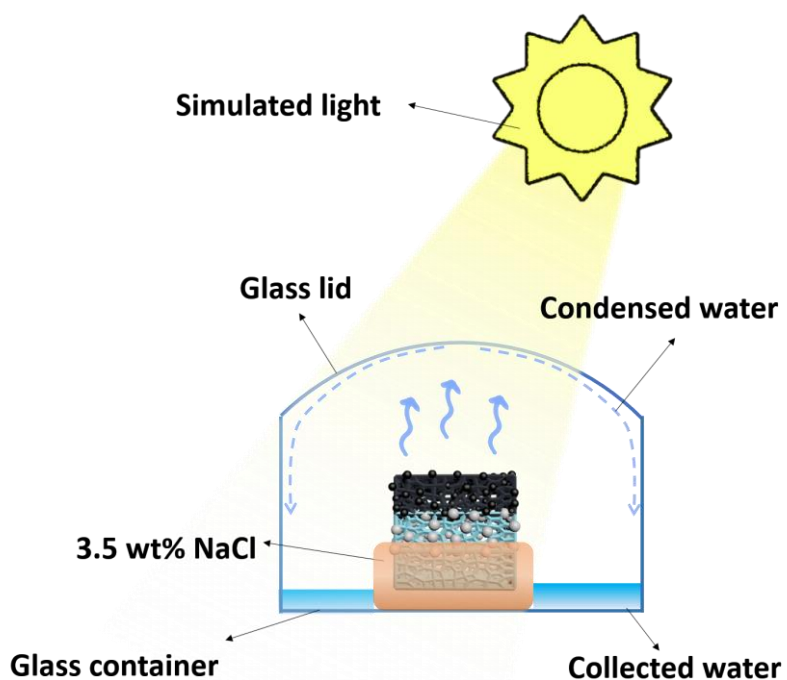
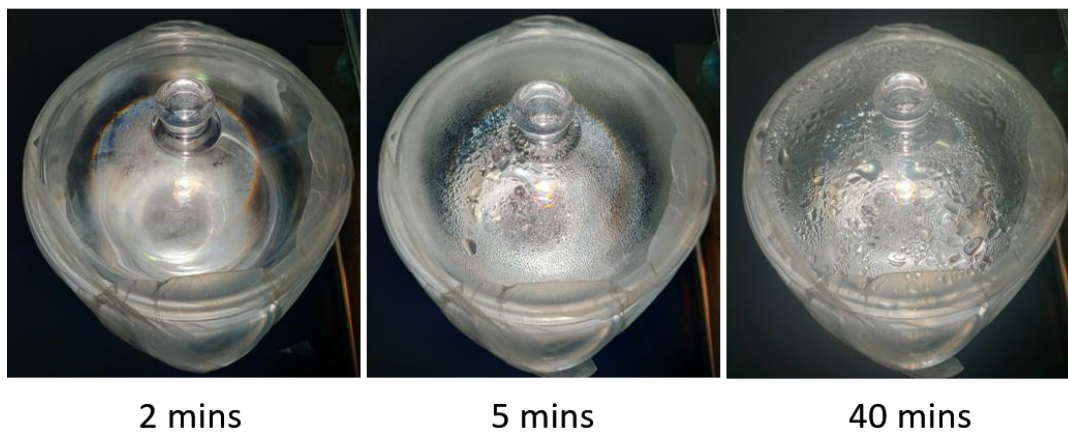**Figure S11** The schematic diagram of the self-made device.

2 mins   5 mins   40 mins

Figure S12 Digital photos of evaporation device during evaporation.

Table S1 Vaporization enthalpy of specimens according to DSC.

Samples	H_2O	HCE-T_0	HCE-T_1	HCE-T_2	HCE-T_3
Vaporization enthalpy/ J g^{-1}	2170	1806	1650	949	1600

Table S2 The summary of calculation of solar evaporation efficiency

Sample	PCA	HCE-T_0	HCE-T_1	HCE-T_2	HCE-T_3
Vaporization enthalpy/ J g^{-1}	2019	1806	1650	949	1600
$r_{aerogel}$/ kg m^{-2} h^{-1}	1.0919	1.6023	1.8762	3.1762	2.0738
r_{dark}/ kg m^{-2} h^{-1}	0.05747	0.07754	0.07408	0.07571	0.05205
r_{net}/ kg m^{-2} h^{-1}	1.03443	1.5248	1.80212	3.1004	2.02175
η/%	58.02	76.49	82.57	81.75	89.82

Reference

[1] J. Sun, B. An, K. Zhang, M. Xu, Z. Wu, C. Ma, W. Li, S. Liu, *J. Mater. Chem. A*, 2021, 9, 24650.

[2] C. Liu, K. Hong, X. Sun, A. Natan, P. Luan, Y. Yang, H. Zhu, *J. Mater. Chem. A*, 2020, 8 (25), 12323-12333.

[3] Z. Tahir, S. Kim, F. Ullah, S. Lee, J.-h. Lee, N.-W. Park, M.-J. Seong, S.-K. Lee, T.-S. Ju, S. Park, J.-S. Bae, J.I. Jang, Y.S. Kim, *ACS Appl. Mater. Interfaces*, 2020, 12, 2490-2496.

[4] Y. Li, T. Gao, Z. Yang, C. Chen, W. Luo, J. Song, E. Hitz, C. Jia, Y. Zhou, B. Liu, B. Yang, L. Hu, *Adv. Mater.* 2017, 29 (26), 1700981.

[5] W. B. Monosmith, and G. E. Walrafen, *J. Chem. Phys.* 986, 81, 669.

[6] F. Zhao, X. Zhou, Y. Shi, X. Qian, M. Alexander, X. Zhao, S. Mendez, R. Yang, L. Qu, G. Yu, *Nat. Nanotechnol.* 2018, 13, 489-495.

[7] L. Hao, N. Liu, H. Bai, P. He, R. Niu, J. Gong, *J. Colloid Interface Sci.* 2022, 608, 840-852.